Journal Pre-proof

Influence of the $BaTiO_3$ addition to $K_{0.5}Na_{0.5}NbO_3$ lead-free ceramics on the vacancy-like defect structure and dielectric properties

A. Prado Espinosa, L. Ramajo, F. Rubio-Marcos, C. Macchi, A Somoza, M. Castro

PII: S0955-2219(20)30829-3

DOI: https://doi.org/10.1016/j.jeurceramsoc.2020.10.016

Reference: JECS 13644

To appear in: *Journal of the European Ceramic Society*

Received Date: 27 May 2020

Revised Date: 4 October 2020

Accepted Date: 9 October 2020

Please cite this article as: { doi: https://doi.org/

Influence of the $BaTiO_3$ addition to $K_{0.5}Na_{0.5}NbO_3$ lead-free ceramics on the vacancy-like defect structure and dielectric properties

A. Prado Espinosa[a], L. Ramajo[a], F. Rubio-Marcos[b,c], C. Macchi[d], A Somoza[d], M. Castro[a,*]

[a] Institute of Research in Materials Science and Technology (INTEMA), Av. Colón 10850, Mar del Plata B7606BWV, Argentina.

[b] Electroceramic Department, Instituto de Cerámica y Vidrio, CSIC, Kelsen 5, 28049 Madrid, Spain.

[c] Escuela Politécnica Superior. Universidad Antonio de Nebrija, Pirineos 55, 28040, Madrid, Spain

[d] Instituto de Física de Materiales Tandil – IFIMAT (UNCPBA) and CIFICEN (UNCPBA-CICPBA-CONICET), Pinto 399, (B7000GHG) Tandil, Argentina

*Author to whom correspondence should be addressed Email: mcastro@fi.mdp.edu.ar

Highlights

- A progressive structural evolution from Orthorhombic to Tetragonal crystal symmetry of lead-free KNN doped with $BaTiO_3$ ceramics; *i.e.* (100-*x*)KNN-*x*BT ($0\% \leq x \leq 7\%$) was associated with the coexistence of O and T phases.

- Ba^{2+} ions occupy the A-sites of the perovskite KNN-based ceramics structure, while Ti^{4+} ions replace the Nb^{5+} ions at the B-sites producing a distortion of the orthorhombic crystal symmetry.
- Positron lifetime annihilation spectroscopy made it possible to reveal the nature and structure of the vacancy-like defects created during the phase transition.

Abstract

A study on the induced changes in the vacancy-like defect structure and the dielectric properties of $K_{0.5}Na_{0.5}NbO_3$ ceramics by the addition of different amounts, between 0% and 7%, of $BaTiO_3$ is presented. The samples were prepared by a mechanochemically activated solid-state reaction method. The structural evolution due to the orthorhombic to the tetragonal phase transition of the KNN doped samples was followed using X-ray diffraction and Raman spectroscopy. The use of positron annihilation lifetime spectroscopy allowed to identify the defect structure at sub-nanometric scale and the nature of the vacancy-like defects generated by the phase transition. The obtained results are discussed considering the lattice symmetry change and the defects structure formed due to the replacement of alkaline and niobium ions by barium and titanium ones. Additionally, changes in the dielectric properties are discussed in terms of the structural modifications of the different KNN-based ceramics involving different kinds of vacancy-like defects.

Keywords: $(K,Na)NbO_3$; $BaTiO_3$; positron annihilation spectroscopy; dielectric properties; point defects

1. Introduction

Lead zirconate-titanate ceramics ($Pb(Zr_{1-x}Ti_x)O_3$ - PZT) are the most widely used and studied piezoelectric materials for applications such as actuators, sensors, transducers, or vibrators [1,2]. However, the use of lead-based ceramics has caused serious environmental problems due to the high toxicity of lead oxide [3]. Consequently, there is an increasing request for the use of environmentally-friendly lead-free ceramics in piezoelectric devices [4]. As an alternative, potassium sodium niobate ceramics ($K_{0.5}Na_{0.5}NbO_3$ - KNN) have attracted the attention due to their high Curie temperature (T_C), good electrical properties, and environmentally friendly nature [5,6]. Moreover, KNN ceramics present a morphotropic phase boundary that increases dielectric properties [7]. This transformation is influenced by the replacement of some of the A or B cations of the perovskite-like structure (ABO_3) modifying, consequently, the Curie temperature and the piezoelectric constant [8,9]. Regardless of having promising properties, there are some problems associated with the KNN ceramics during processing. One major problem is the volatilization of alkali elements at the sintering temperatures, where oxygen vacancies are created increasing the electronic conductivity of the ceramics [10,11].

To modify final properties, several solid solutions have been investigated [11-13]. In $(1-x)K_{0.5}Na_{0.5}NbO_3$-$xBaTiO_3$ (KNN-BT) ceramics, BT diffuses into the KNN lattice to form a solid solution [14-18]. Subsequently, barium ions replace sodium or potassium ions at the A-sites whereas titanium ions are located at the B-sites occupied by niobium ions. Guo *et al.* [15] noted that for 4%BT, KNN-BT ceramics still retain an orthorhombic structure. However, for a concentration of 6%BT the crystalline symmetry exhibits a small tetragonal distortion, indicating that the morphotropic phase edge is established. For BT compositions higher than

20%, the authors reported another phase transition corresponding to a cubic symmetry where a significant decrease in the piezoelectric properties was detected.

It is known that KNN-based ceramics in the range between room temperature (RT) and 500°C display two phase transitions, attributed to a phase transformation from the orthorhombic phase to the tetragonal one; and then, to the paraelectric phase [19]. Consequently, dielectric curves show marked peaks revealing these phase transformations with the temperature, which are sensitive to changes in the composition of the system. It was reported that in KNN-$SrZrO_3$ solid-solutions, as the concentration of the second component increases, the peak of the dielectric permittivity corresponding to the ferroelectric tetragonal to the paraelectric cubic structure shifts to lower temperatures and, besides, it becomes much broader than those obtained for pure KNN ceramics [20]. Dielectric studies reveal that $0.97(K_{0.5}Na_{0.5})NbO_3–0.03(Ba_{0.6}Sr_{0.4})_{0.7}Bi_{0.2}TiO_3$ ceramics show a broad dielectric peak with a permittivity maximum near 2000 and a low dielectric loss (*i.e.*, tan δ) [20]. Liu *et al*. [21] found temperature-stable dielectric properties in the $0.86(K_{0.5}Na_{0.5})NbO_3$-$0.14SrZrO_3$ solid solution ceramics with high dielectric permittivity (ε = 2310) and a low dielectric loss sustained in a broad temperature range (from −55°C to 201°C). These authors detected that Sr and Zr elements exhibited an inhomogeneous distribution from the shell to the core within grains and attributed these duplex grain microstructures to the observed temperature-stable dielectric properties. Liu *et al*. [22] also determined that KNN-NbZn ceramics displayed both high permittivity and low dielectric loss (tan δ) in a wide temperature range (from 20 °C to 500 °C). They concluded that the dopants enter into the lattice positions modifying the symmetry of the crystal structure and the microstructural morphologies. Also, the observed thermal stability dielectric performance is due to the orthorhombic to tetragonal and

tetragonal to cubic phase transition peaks suppression, indicating an evolution from a sharp to a diffuse phase transition.

Positron annihilation spectroscopy (PAS) is a well-recognized, non-destructive nuclear technique for studying open volume defects in solids [23]. In particular, PAS has demonstrated to be a powerful tool to investigate the presence of vacancy-like defects in metals and semiconductors [24,25].

Some authors of the present work have used positron annihilation lifetime spectroscopy (PALS), one of the experimental variants of PAS, to characterize vacancy-like defects in $BaTiO_3$-based ceramics. In particular, in a first work, it was possible to characterize and quantify vacancy-like defects in $BaTiO_3$ single crystals submitted to thermal cycles including the critical temperature T_c of the ferroelectric–paraelectric transition [26]. A few years later, the authors used PALS and electron paramagnetic resonance to study the compensation mechanisms in donor-doped $BaTiO_3$-based ceramics [27]. The results obtained made it possible to conclude that vacancy-like defects present in the different $BaTiO_3$–based specimens were dependent on the type of additive. Besides, in each case, it was proposed a relationship among the doping levels and the defect structures.

In general, from the positron lifetime spectra decomposition several lifetime components can be obtained; each of them is characterized by a lifetime τ_i and an associated intensity I_i. The state *i* can be the delocalized one in the lattice (bulk state), or localized states at different defect sites in which positrons become trapped and annihilated. In this last case, the value of the positron lifetime reflects the size of the open volume associated with the defect in which positrons are annihilated; increasing lifetime values indicate that positrons become trapped in bigger open volumes.

In the present work, a systematic analysis of the structural at the micro- and nano-scale and the dielectric properties of the $K_{0.5}Na_{0.5}NbO_3$ ceramics with the addition of different amounts of $BaTiO_3$ is presented. Firstly, the structural characterization of the different samples is presented. Toward this aim, the phase transition from orthorhombic to tetragonal symmetry due to the addition $BaTiO_3$ to pure $K_{0.5}Na_{0.5}NbO_3$ was obtained using XRD and Raman spectroscopy. Besides, the morphology and the grain size distribution are shown. The nature of the vacancy-like defects induced by the structural evolution of the KNN-based ceramics during the orthorhombic to the tetragonal phase transition, as a consequence of the BT addition, was investigated using PALS. On the other hand, the influence of the BT doping on the dielectric properties of the KNN ceramics is analyzed and discussed. Finally, a summary and a joint discussion of the main results obtained are presented.

2. Experimental

$(100\text{-}x)K_{0.5}Na_{0.5}NbO_3\text{-}xBaTiO_3$ ceramics with (x = 0, 3, 4, 5, 6 and 7) ceramics were synthesized by the conventional solid-state reaction method. For the synthesis, all reactants (Na_2CO_3 (Biopack 99.5%), K_2CO_3 (Cicarelli 99.99%), Nb_2O_5 (Aldrich 99.9%), $BaCO_3$ (Merck 99%) and TiO_2 (Aldrich 99.9%)) were mechanochemically activated, using zirconia balls in an alcoholic medium for 3 h, in a planetary mill (Fritsch, Pulverisette 7, 1450 rpm) and subsequently heat-treated at 800°C for 2 h. The powders obtained were uniaxially pressed into discs and sintered at 1150°C for 2 h. To study the influence of $BaTiO_3$ addition on the defect's formation in the perovskite and to avoid possible interactions, sintering aids were not added in the samples. The nomenclature of sintered samples is detailed in Table 1.

Sample	KNN	KNN-3BT	KNN-4BT	KNN-5BT	KNN-6BT	KNN-7BT
%BT	0.0	3.0	4.0	5.0	6.0	7.0
%KNN	100.0	97.0	96.0	95.0	94.0	93.0
ρ (g/cm^3)	4.28	4.10	4.10	4.07	3.90	3.80
Densification (%)	95.3	90.7	90.3	89.5	85.5	83.2

Table 1. Nomenclature, measured density (ρ) values and densification (%) of the KNN-xBT sintered samples.

Structural analyses were performed using X-ray diffraction patterns (XRD) employing a PANalytical, X'pert Pro with CuK_α radiation whereas Raman spectroscopy studies were carried out using a Renishaw In Via Reflex multichannel microspectrometer. Structural refinement was performed using a tetragonal symmetry ***(T, P4mm)*** and an orthorhombic symmetry ***(O, Amm2).*** The relative volume fractions can be calculated by using the integrated intensities of degenerate reflections, such as the tetragonal (002) and (200), orthorhombic (022), and (200) peak, respectively, obtained from line profile analysis [28]. Peaks positions were fit assuming a Lorentz peak shape (*more information about the evolution of the phase volume fraction as a function of the $BaTiO_3$ content is given in the* ***Supplementary Information SI.1***).

Relative density values were determined using the Archimedes´ method whereas the theoretical density (ρ^t) for each composition was calculated by mixtures´ law, considering the density of the $(K_{0.5}Na_{0.5})NbO_3$ and $BaTiO_3$ pure phases 4.49 g/cm^3 (ICSD 186341) and 6.02

g/cm^3 (ICSD 72-0128), respectively. Microstructural characterization was evaluated using a field emission scanning electron microscope (FE-SEM, Sigma, Zeiss, Germany) on fractured samples. The average grain size and grain size distributions were determined from FE-SEM micrographs by an open-source image-processing program (ImageJ), considering more than 150 grains in each measurement.

For dielectric characterization, electrodes were painted with silver paint. Dielectric measurements were carried out as a function of the temperature (from 25°C to 500°C) and in the frequency range of 100 Hz to 1 MHz using an impedance analyzer (LCR meter HP4284A).

PALS spectra were obtained using a *Positron Lifetime Picosecond Timing System ORTEC* ® with a time resolution of 210ps in a collinear geometry. As a positron source, a 10µCi sealed source of ^{22}NaCl (Radionuclides Product Number: NEZ081 produced by PerkinElmer) deposited onto two thin Kapton foils (7.5µm thick) sandwiched between two identical samples was used. The spectra were acquired at RT and, typically 1.5-2x10^6 counts per spectrum were collected. The lifetime values reported in this work for each sample are at least an average of 10 measurements in the same experimental conditions. After subtracting the background and the source contribution, positron lifetime spectra were analyzed using the LT10 code [29].

3. Results and discussion

3.1 *Microstructural characterization and perovskite structure compounds*

Fig. 1(a) shows the diffraction patterns of the KNN-BT system in the range of the BT compositions studied. In general, the results reveal the existence of the perovskite structure without the presence of secondary phases. To analyze the (022) and (200) diffraction peaks

located at 45°<2Θ<47° and to determine the integral angular and wide positions, the patterns were adjusted using a Lorentz peak function. The corresponding settings are shown in Fig. 1(b). The phase structure for varying BT concentrations is judged by the characteristic (002)/(200) diffraction peaks. Both the splitting of the (002) and (200) diffraction peaks, as well as the intensity changes caused by the addition of $BaTiO_3$ to the $K_{0.5}Na_{0.5}NbO_3$, indicate that there is an evolution in the orthorhombic symmetry (O), characteristic of KNN at RT, to a tetragonal one (T) for the (100-x)$K_{0.5}Na_{0.5}NbO_3$-x$BaTiO_3$ system (see Fig. 1(c)). Specifically, for the ceramic with x = 0, the crystal symmetry is exclusively the O-phase; while in the compositional range $3 \leq x \leq 6$, all samples presented a polymorphic behavior, which is associated with the RT coexistence of the tetragonal (***T, P4mm***) and orthorhombic ***(O, Amm2)*** symmetries. It should be highlighted that this polymorphic behavior shows a clear evolution with the progressive addition of BT. First, in the composition range $3 \leq x \leq 4$ at a RT coexistence of ***O-T*** phases is observed, the peaks associated with ***O*** symmetry being most relevant (see Fig. 1(c)). By contrast, a different trend is detected for the compositions with higher BT contents (*i.e.*, $5 \leq x \leq 6$). In this last compositional range, the peaks associated with the tetragonal symmetry are more relevant than in the ceramics with low BT contents, which implies a stabilization of the tetragonal symmetry (see Fig. 1(c)). Finally, for the sample with the highest BT addition (*i.e.*, x = 7), the tetragonal symmetry is only registered. (*More information about the phase volume fractions depending on the BT content is given in the* ***Supplementary Information SI.1***).

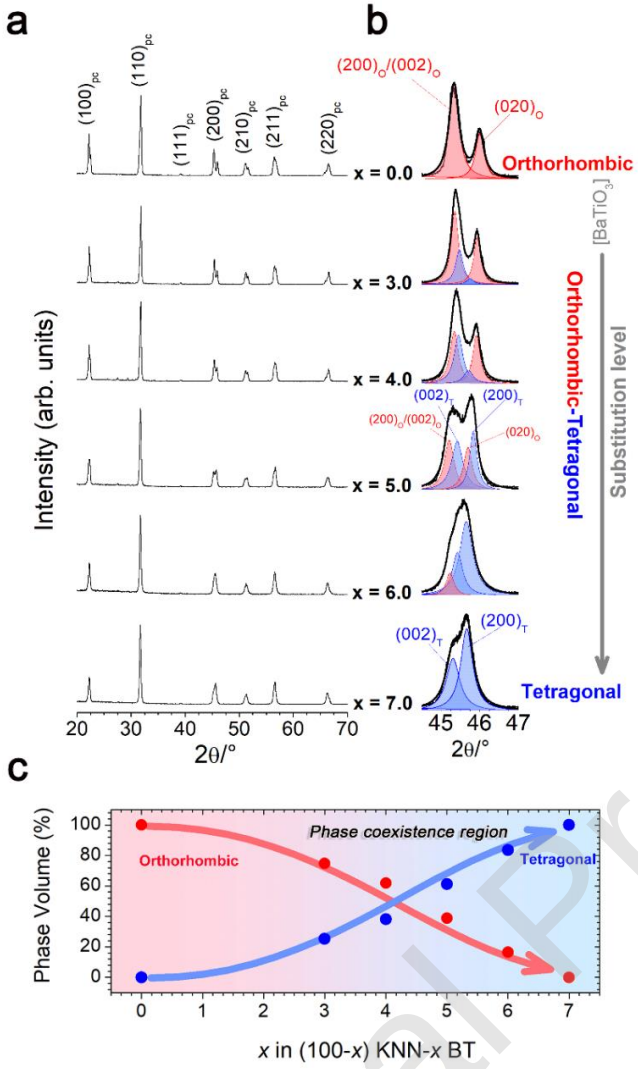

Figure 1. X-ray diffraction patterns of the different (100-x)$K_{0.5}Na_{0.5}NbO_3$-x$BaTiO_3$ samples. In **panel (**a**)**, the patterns are presented following the BT additions between x=0% (top) → x = 7% (bottom). The panel (b**)** shows a detail of the XRD diffraction pattern in the 2θ range from 44.5º to 47º of the (100-x)$K_{0.5}Na_{0.5}NbO_3$-x$BaTiO_3$ ceramics. The patterns with $3 \leq x \leq 6$ were fitted using a sum of 4 Lorentzian peaks, 2 tetragonal peaks (represented in blue color) plus 2 orthorhombic ones (in red color) of the perovskite phase. In the case of the ceramics with x = 0% and x = 7%, the patterns were fitted using in each case the sum of 2 Lorentzian peaks, 2 orthorhombic peaks (represented in red color) and 2 tetragonal ones. In panel (c**)**, the volume fraction of the *T* and *O* phases as a function of the BT content is shown. (More details on this figure are given in the text).

Fig. 2(a) shows the Raman spectra of the KNN-BT system for all compositions under study. The figure shows that the Raman spectra of the (100-x)KNN-xBT systems have the typical vibration modes corresponding to the perovskite phase [28,30,31]. The observed modes in the range of 0–200 cm^{-1} are classified as the translational modes of the mixed perovskite A-site, including Na^{+}, K^{+}, and Ba^{2+} cations, whereas the internal vibrational modes in the range of 200–700 cm^{-1} are related to the NbO_6-octahedra vibrations [32]. v_1, v_2, and v_5 modes are the breathing or bending modes of the oxygen octahedra, whereas the v_3 and v_4 modes are the stretching and bending modes of the Nb-O bond [33]. It can also be seen that BT increase induces small changes in the internal modes associated with the octahedron of NbO_6 and leads to the modification of the Raman spectra. Changes in the position of the υ_1 mode located at 620 cm^{-1}, corresponding to the vibration contraction of the NbO_6 octahedron due to the difference of the Nb-O bonds, are observed, a band broadening and the movement of the υ_2 mode to a lower position of this mode are detected (see Fig. 2(b)). These shifts can be related to changes in the perovskite structure, produced by the incorporation of titanium (ionic radius 0.605 Å), which induces a distortion in the angles of the O-Nb-O bond [28]. The increase in the strength of the union between the Nb^{5+} (ionic radius 0.65 Å) and its coordination oxygen when the shortening of the link distance occurs and, consequently, the corresponding oxygen octahedral of NbO_6 changes their vibrations [34,35]. At the same time, these results added to those obtained by XRD patterns would indicate that Ba^{2+} ions occupy the A-sites of the structure, and the Ti^{4+} ions replace the Nb^{5+} ions at the B-sites, resulting in the distortion of the perovskite structure. This distortion induces a change in the local symmetry of the vibrations and the deformation of the NbO_6 octahedron [34]. Consequently, the observed Raman bands broadening can be associated

with the structural evolution from orthorhombic to tetragonal symmetry where the disorder degree is rising with $BaTiO_3$ addition.

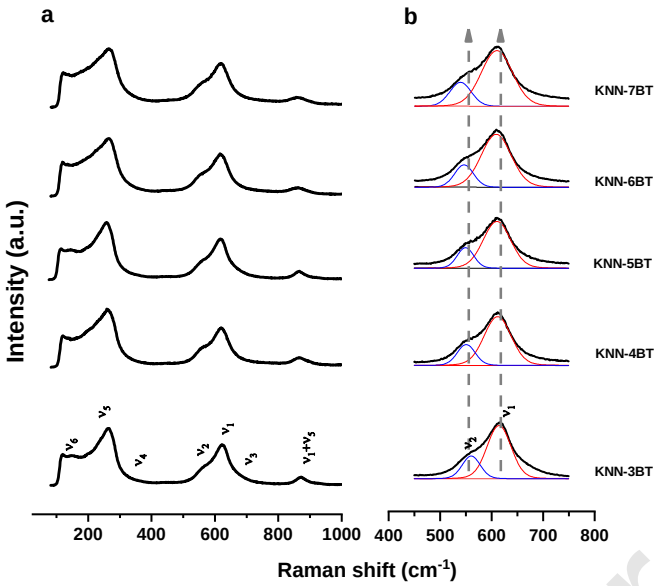

Figure 2. (a) Raman spectra for the different KNN-xBT, 3.0≤x≤7.0 ceramics samples. (b) Amplified Raman spectra fitted by the sum of 2 Lorentzian peaks, ascribed to the Eg (υ_2) and A1g (υ_1) corresponding to Raman modes of the perovskite phase.

Figs. 3(a)-3(e) show the FE-SEM images of the samples corresponding to the KNN-BT system, sintered at 1150°C for 2 h, where the respective grain distribution diagrams are included. All samples retain the typical microstructure with cubic and faceted grains characteristic of the KNN ceramics. From the images, a grain size diminution for increasing BT content can be observed. These results are in agreement with those reported in the literature [36-38]. Specifically, the medium grain size decreases from 2.4 μm to 0.06 μm when the BT content is increased from 3% to 7%. These microstructural changes are accompanied by a remarkable reduction in the density values (see Table 1). Unfortunately, the densification degree of these samples is not high. For a better densification plasma spark

sintering [39], hot-pressing [**7**], the incorporation of additives (such as CuO, ZnO, SnO_2, CeO_2, MnO_2, WO_3, TiO_2 [40,41] or a stable glass [42]) could be analyzed in future studies. Additionally, these changes in the grain size with $BaTiO_3$ addition could also contribute to the observed broadening of the Raman spectra in Figure 2, especially for the higher additions (6% and 7%).

The better homogeneity and density of the grains in the ceramics with the KNN-4BT composition than KNN-3BT suggest that the presence of a possible polymorphic phase boundary (PPB) (orthorhombic-tetragonal phase) would increase the mass transport, resulting in more homogeneous grain growth. It is noted that alkaline volatilization, typical of KNN-based ceramics, did not cause the formation of secondary phases in this system, nor the apparent formation of the liquid phase during the sintering process.

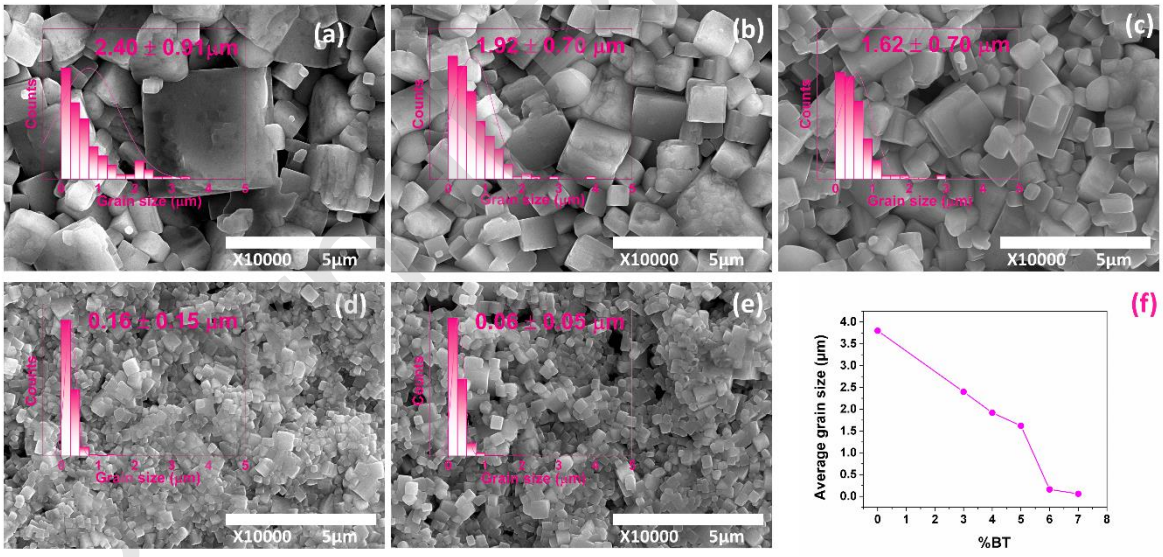

Figure 3. FE-SEM images of KNN-3BT (a), KNN-4BT (b), KNN-5BT (c), KNN-6BT (d), and KNN-7BT (e) ceramic samples. Additionally, the evolution of the grain size as a function of the BT addition is shown (f).

Different authors have reported that in perovskite structure compounds, to maintain

charge neutrality, oxygen vacancies must be generated [43,44 ~~39,40~~]. In particular, in KNN-based ceramics, due to the volatile nature of the alkaline elements during high-temperature processing, cationic and oxygen vacancies are also generated by oxygen losses in high-temperature treatments [43 ~~39~~]. Using the Kroger-Vink notation, the defects generated by the volatile elements or oxygen loss can be expressed according to the following equations:

$$Na_{Na} + e' \rightarrow Na + V'_{Na} \quad (1)$$

$$K_K + e' \rightarrow K + V'_K \quad (2)$$

$$O_O \rightarrow \frac{1}{2}(O_2) + V_O^{\bullet\bullet} + 2e' \quad (3)$$

Additionally, due to the substitution produced at the A and B sites of the perovskite by the incorporation of BT, new oxygen and cationic vacancies are generated, as detailed in Eqs. (4), (5) and (6). In the case of the replacement of Na^+ and K^+ by Ba^{2+} ions, it is expected a preferential replacement at the K^+ sites due to the ionic radii similarity.

$$2TiO_2 + 2Nb_{Nb} + O_O \rightarrow 2Ti'_{Nb} + V_O^{\bullet\bullet} + Nb_2O_5 \quad (4)$$

$$BaO + 2K_K \rightarrow Ba_K^{\bullet} + V'_K + K_2O \quad (5)$$

$$BaO + 2Na_{Na} \rightarrow Ba_{Na}^{\bullet} + V'_{Na} + Na_2O \quad (6)$$

3.2 *Defect structure*

To go deeper into the analysis of the possible defects stabilized in the KNN-BT ceramics, PALS studies were carried out. As an example, in Fig. 4 two typical spectra of those obtained measuring our samples are shown; specifically, and for the sake of clarity, the PALS spectra

chosen correspond to the pure KNN and KNN-6%BT samples. Depending on the sample, PALS spectra could be satisfactorily fitted using up to three discrete lifetime components (specific *information regarding the analysis of PALS spectra is given in the* ***Supplementary Information SI.2*****).** Furthermore, in all measured spectra, a long-lived lifetime of about 1700-2000ps with an associated intensity <0.5% was found. Taking into account the small value of the intensity of this lifetime, this lifetime component was not considered for further discussions.

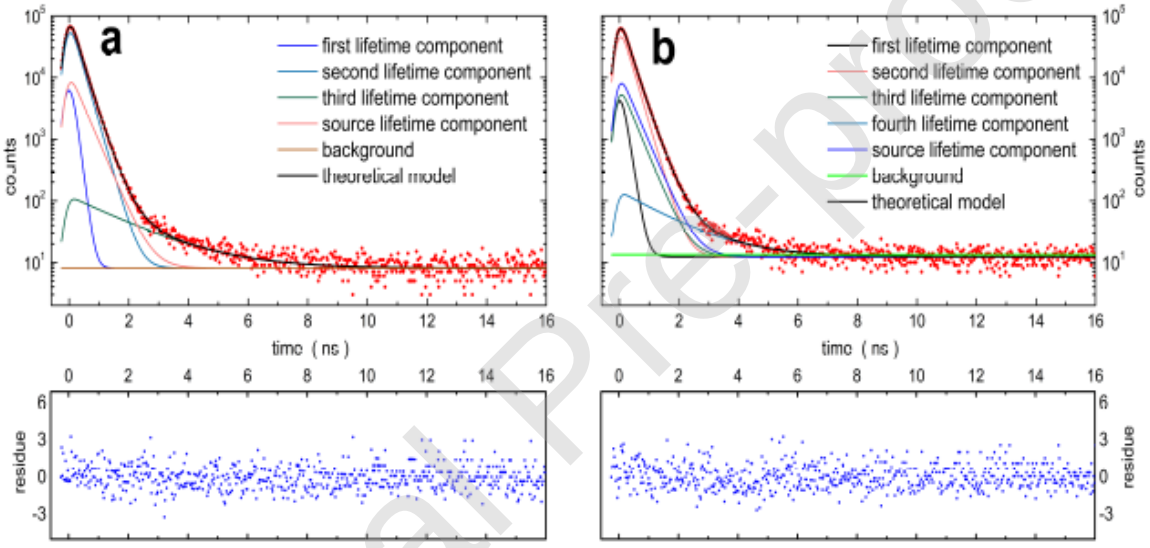

Figure 4. PALS spectra of a pure KNN (panel **a**) and KNN-6%BT (panel **b**) samples. For the sake of clarity, only two spectra representing the pure and the doped samples are presented.

As can be seen in Table 2, from the PALS spectra measured for the pure KNN sample two lifetime components were obtained. There exists a dominant lifetime component characterized by a lifetime of 265±2ps and associated intensity of ~80%, and another component that has a shorter lifetime of 152±5ps.

Sample (%BT)	τ_1 (ps)	I_1 (%)	τ_2 (ps)	I_2 (%)	τ_3 (ps)	I_3 (%)
0	152 ± 5	20 ± 1	265 ± 2	80 ± 1		
3	108 ± 6	7 ± 2	262 ± 3	85 ± 2	363 ± 10	8 ± 1
4	105 ± 6	5 ± 1	263 ± 2	86 ± 1	365 ± 10	9 ± 1
5	120 ± 6	10 ± 4	266 ± 2	77 ± 4	370 ± 10	13 ± 2
6	125 ± 6	9 ± 1	267 ± 2	77 ± 1	365 ± 10	14 ± 1
7	209 ± 3	39 ± 2	295 ± 2	60 ± 2		

Table 2. Characteristic positron lifetimes and their associated intensities obtained from the decomposition of PALS spectra.

For the KNN sample doped with different amounts of BT up to 6%, in the spectra decomposition a third-lifetime component (τ_3, I_3) was observed. In this doping concentration range, the second and third-lifetime values are almost constant, within the experimental scatter, and their values are τ_2~ 265ps and τ_3 ~368ps, respectively. Besides, the corresponding intensities associated with these lifetimes change depending on the doping concentration.

In the case of the samples of KNN with BT addition up to 4%, the intensity I_2 grows from 80% to 86%. In the concentration BT range between 4% and 6%, I_2 decreases to 77%; while, I_3 grows from 0% to 14%. For the highest doping of the KNN system; that is, 7% BT the decomposition of the PALS spectra could satisfactorily be decomposed into two lifetime components.

When studying materials having complex structures in which several kinds of defects can be considered to exist, theoretical calculations of positron states are very useful to interpret the measured positron lifetimes (see for example Refs. [45,46 ~~41,42~~]).

In this work, we have used the simplest calculation scheme to obtain theoretical positron lifetimes for the bulk and for different vacancy states that could be present into the pure KNN structure. Specifically, positron lifetimes were calculated using the density-functional theory (DFT) within the so-called standard scheme [47 ~~43~~]. Toward this aim, a rigid lattice was considered and to calculate the effective lattice electron density the atomic superposition approximation method (ATSUP) implemented in the Doppler program included in the MIKA package [48 ~~44~~] was employed. For the electron-positron correlation, the local-density approximation (LDA) was used employing the Boronski and Nieminen parameterization [49 ~~45~~], with a correction for an incomplete positron screening [50 ~~46~~] using the dielectric permittivity value experimentally determined in the present work at RT and 1 MHz for the KNN system, $\varepsilon_\infty = 299$.

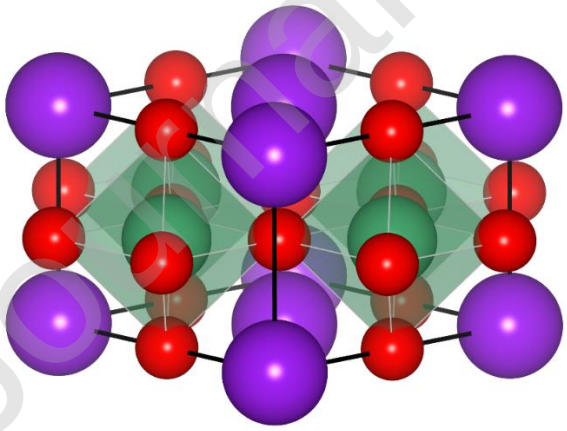

Figure 5. Orthorhombic KNN unit cell. In the figure, Na and K atoms are represented in violet, Nb atoms in green, and O atoms in red.

To model the undefected KNN lattice, we have used an orthorhombic unit cell with 10 atoms, presented in Fig. 5 (*Amm2*nro 38 space group) [51 ~~47~~] with the experimentally determined lattice parameters: a=3.95Å, b=5.68Å, and c=5.65Å [52,53 ~~48,49~~].

On the other hand**,** the defect states were modeled using a supercell of 640 atoms (4×4×4 replication of the unit cell depicted in Fig. 5). In Figs. 6 and 7, the vertical and horizontal cross-sections of the supercell modified by the creation of different vacancy-like defects in the modeled KNN supercell are presented, respectively. In particular, as can be seen in Fig. 6 an oxygen vacancy ($V_O, labeledA$) was created by removing an O atom; a potassium vacancy (V_K) by removing a K atom and a sodium vacancy (V_{Na}) by removing a Na atom, to these two kinds of vacancies was assigned the same $labelB$. Besides, in this figure different K-O vacancy-complexes can be observed: the $V_K + V_O$ divacancy, labeled C; the $V_K + 2V_O$ trivacancy labeled D, and the pentavacancy $V_K + 4V_O$ labeled E, which were modeled removing 1, 2 and 4 O atoms nearest-neighbors to the V_K, respectively. In Fig. 7, it can be seen a niobium vacancy ($V_{Nb}, labeledA$) created by removing a Nb atom; and a Nb-O vacancy-complex ($V_{Nb} + V_O$ divacancy, labeled B created removing the O atom nearest-neighbor to the V_{Nb}.

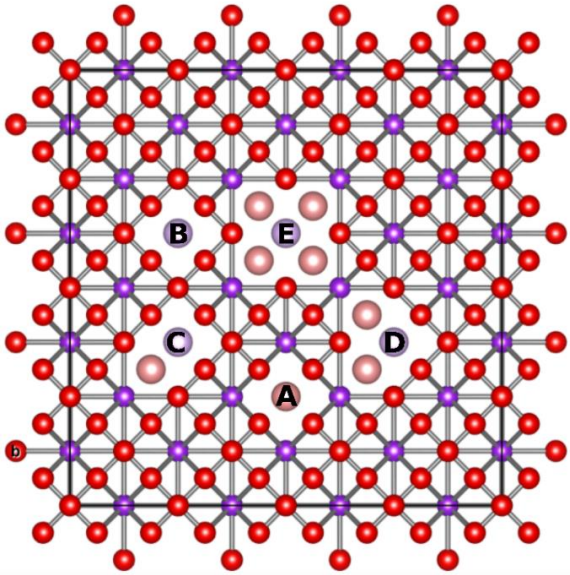

Figure 6. Vertical cross-section of the orthorhombic KNN supercell used for the calculation of positron lifetimes. In this figure, the different vacancy-defect states simulated in the present work can be identified: **(A)** V_O; **(B)** V_K (or V_{Na}); **(C)** $V_K + V_O$; **(D)** $V_K + 2V_O$ divacancy; and **(E)** $V_K + 4V_O$ pentavacancy. In the figures, the Na (or K) atoms are represented in violet and O atoms in red. Light violet and light red spheres represent a missing Na (or K) and O atom, respectively.

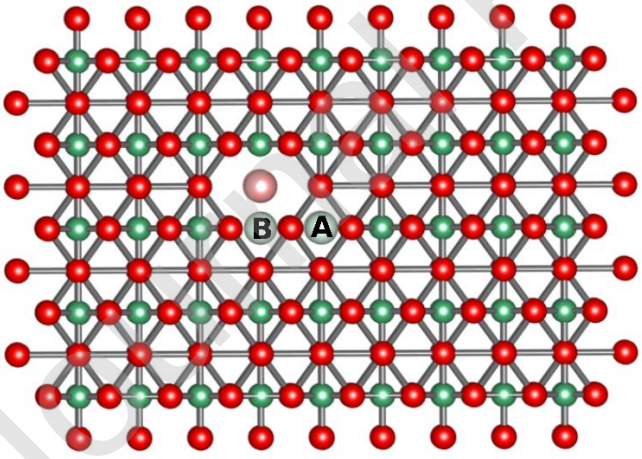

Figure 7. Horizontal cross-section of the orthorhombic KNN supercell used for the calculation of positron lifetimes. In this figure, the different vacancy-defect states simulated in the present work can be identified: **(A)** V_{Nb} and **(B)** $V_{Nb} + V_O$ divacancy. *In the figures, Nb atoms are represented in green and O atoms in red. Light green and light red spheres represent a missing Nb and O atom, respectively.*

As a first approach, for all calculations presented in this work, non-ionic relaxations were considered. Besides, all defect states were assumed to be in their neutral state. The results obtained are reported in Table 3. From the analysis of the results presented in the table, the positron lifetime calculated for a V_O is barely 2% higher than that calculated for the bulk (τ_b). It must be stressed that in metal-oxide perovskites (ABO_3), an isolated oxygen vacancy is considered as a shallow trap and, therefore, the V_O can hardly trap positrons. On the contrary, A- and B-sites vacancies are deeper positron traps and, consequently, they can be detected by positrons [54,55 ~~50,51~~].

Positron state	positron lifetime τ (ps)
bulk	157
V_O	161
V_{Nb}	183
V_K	253
V_{Na}	254
$V_{Nb} + V_O$	209
$V_K + V_O$	259
$V_K + 2V_O$	266
$V_K + 4V_O$	280

Table 3. Theoretical positron lifetimes for a KNN structure and various defects states (see text).

From our results, it is clear that positron lifetime values are strongly dependent on the site of the lattice in which a vacancy is located. In such a case, from now on we will refer to a K or Na vacancy as an A-site vacancy (V_A) and in the case of the Nb vacancy as a B-site vacancy (V_B). When considering a V_B, its positron lifetime is ~17% higher than that calculated for the bulk, while the positron lifetime for a V_A is approximately 60% higher than τ_b.

The important difference between the positron lifetime annihilated in V_A and τ_b makes it possible to conclude that this type of vacancy should be detected. Furthermore, when oxygen vacancies are aggregated to a cation vacancy to form metal-oxygen vacancy complexes the results of the positron lifetimes are higher than those obtained for an isolated metal vacancy. It must be mentioned that the calculated lifetime for the $V_A + V_O$ divacancy is only slightly higher (~2%) than that obtained for an isolated V_A; besides, in the case of $V_B + V_O$, its positron lifetime is ~15% higher than that obtained for the V_B. Our results are in qualitatively good agreement with those reported in the literature of positron lifetimes calculated for vacancy states in other kinds of perovskite systems (see for example Refs. [54,55 ~~50,51~~]).

Based mainly on the positron lifetime values obtained using *ab-initio* calculations for the different positron states reported in Table 3, an analysis and a discussion of the experimental data reported in Table 2 are given as follows:

(i) Pure KNN sample

It is important to remember that from the analysis of the PALS spectra obtained measuring pure KNN samples a dominant lifetime component of ~265ps with an associated

intensity of ~80% and a short-lived lifetime component of ~152ps and I_1 ~20% is present. To our knowledge, there is only one paper in which the same pure system was studied by PALS [52 ~~48~~], the results reported show a reasonable agreement with those presented here.

Taking into account the lifetime values reported in Table 3, the experimental lifetime τ_2 can be interpreted as the result of positron annihilation in $V_A + V_O$ vacancies complexes. In such a case, positron traps would have a mean size comparable to that formed by two V_O surrounding one A-site vacancy. Besides, the high I_2 value indicates that there is a high concentration of this kind of defect. The assumption of the existence of the mentioned defect seems to be very reasonable since it was reported that in pure KNN the predominant defects should be the K and Na vacancies (see Eqs. (1) and (2)) caused by the volatilization of these elements at high sintering temperatures [56 ~~52~~]. On the other hand, the experimental τ_1 is lower than the calculated τ_b; consequently, it must be considered τ_1 as a reduced bulk lifetime due to positron annihilations in $V_A + V_O$ vacancy complexes, but it cannot be excluded that some positrons could be annihilated in Nb vacancies. It is worth mentioning that in such a complex system, positron annihilation cannot be analyzed using the well-known simple Standard Trapping Model (STM) [23] because there is a variety of defects that can act as effective positron traps. Therefore, it is not possible to get direct information regarding the defect concentration in the pure KNN samples.

(ii) BT-doped KNN samples (up to 6%)

When the KNN samples are doped with BT in the compositional range between 3% and 6%, among the three positron lifetimes components obtained from the decomposition of the PALS spectra, the dominant one is characterized by the same lifetime value, indicating

that in the four samples studied the same kind of vacancy-like defects as those detected in the pure KNN sample is present; specifically, $V_A + V_O$ vacancy complexes.

On the other hand, when analyzing the I_2 evolution for increasing BT doping the analysis can be divided into different stages. Comparing with the reference pure KNN sample, the increase in the I_2 value observed for the KNN samples doped up to 4% BT indicates an increment in the concentration of the vacancy complexes described above. So, such a level of doping would favor the formation of new K and/or Na vacancies complexed with O vacancies (see Eqs. (5) and (6)). For higher BT addition, the I_2 decrease reflects a diminution of the concentration of vacancy complexes. However, as can be seen in Table 2 its concentration is still high enough.

In the case of the third-lifetime component, such a high τ_3 value is similar to those reported for nanostructured systems such as compacted nanocrystalline powders and nanostructured metallic samples [46, 57-60 ~~42, 53-56~~]. In these works, the authors attributed such lifetime values to positron annihilations into point defects with an associated open volume comparable to small vacancy clusters located at the grain boundaries. As reported above, all the samples analyzed in the present point have grain sizes around 1 μm; we also know by the literature [61 ~~57~~] that in polycrystalline samples having similar or bigger grain sizes, the number of positrons annihilating into grain boundaries is almost negligible.

The XRD and Raman spectroscopy results presented in this work indicate that the addition of BT to pure KNN induces a gradual phase transformation from the orthorhombic structure characteristic of pure KNN to a tetragonal one. In particular, in the compositional range between 3% and 6% BT doping, the polymorphic behavior at room temperature is reasonably identified as the coexistence between tetragonal and orthorhombic symmetries,

which is modulated by the BT content, highlighting that the relative volume fraction of the T phase gradually increases while the O-phase content decreases. Taking into account the experimental results obtained in the present work using PALS, XRD and Raman spectroscopy for the (100-x)$K_{0.5}Na_{0.5}NbO_3$-x$BaTiO_3$ (x = 3, 4, 5 and 6) samples; and those reported in the literature from PALS studies on nanocrystalline powders and nanostructured metallic samples [48, 57-60 ~~42,53-56~~] and by Baker *et al.* [62 ~~58~~] from high-resolution XRD and neutron powder diffraction on KNN with different K/Na ratios sample, we could conclude that the high τ_3 value comes from positron annihilations in vacancy-like defects with associated big open volumes located at the orthorhombic-tetragonal phase boundaries.

(iii) KNN-7%BT sample

The results obtained for the sample doped with 7% BT must be analyzed separately from those previously obtained for the other KNN-BT samples due to two reasons:

(i) the sample is in the tetragonal phase; and

(ii) the average grain size is ~60 nm, which is comparable to the typical positron diffusion length in solids, L_+~50-100nm [23].

Consequently, it can be assumed that a large number of positrons easily reach the grain boundaries by diffusion and, then annihilates there [59,61 ~~55,57~~]. Therefore, the dominant lifetime component τ_2 = 295±5ps can be attributed to positron annihilations in vacancy-like defects located at the intergrain regions. The value of the short-lived lifetime component τ_1 = 209±3 ps is higher than that calculated for the free-defect state of pure KNN, τ_b (see Table 3); therefore, this lifetime could be interpreted as an average of different contributions of positron lifetimes arising from positrons annihilated in small vacancy-like defects located in

the intragrain regions with an open volume comparable to mono- or di-cationic vacancies (K and/or Na and/or Nb) and to positron annihilations into the bulk of the sample.

3.3 Dielectric properties

Dielectric properties of the samples corresponding to the system under study are presented in Fig. 8, where changes in the permittivity as a function of the temperature are shown.

From the analysis of the permittivity curves for pure KNN, two-phase transitions were detected. At approximately 196°C, the ferroelectric orthorhombic to the tetragonal phase transition produces a step in the real permittivity *versus* temperature curves, whereas the pronounced maximum close to 400°C reveals the ferroelectric tetragonal to the paraelectric cubic phase transition. Interestingly, these peaks shift to lower temperatures with the addition of barium titanate (for low BT contents); and finally, a broad peak is detected for the highest BT concentrations.

In what follows, the results are discussed according to the BT concentrations. For $3 \leq x \leq 6$, the main real permittivity peak shifts to lower temperatures. The highest value of the dielectric permittivity is observed for the samples containing 3% and it could be the result of a mixed structure of the O-T phases. It is well-known that a mixed structure at a given composition increases the polar nature of the ceramic, which is reflected in an increase of the corresponding polarization [63 ~~59~~]. Consequently, the greater the polarization in a system, the greater the value of its permittivity. For higher BT addition, the broadening of the peak could be due to a lattice disordering or the strain induced by the doping [64 ~~60~~]. Also, the increase of the relative permittivity can be attributed to the decrease grain size with BT addition.

Besides, the low-temperature peak observed in the real permittivity curves shifts from 196°C for pure KNN, to approximately 100°C, 90°C and 60°C for samples with 3%, 4% and 5% of BT addition, respectively. Taking into account that this low-temperature peak is related to the orthorhombic to tetragonal structural transition, the shift in the temperature observed for this peak is indicative of the KNN structural transitions with the barium titanate addition. Guo *et al.* [15] reported that for the same KNN-based ceramic with BT additions until 4%, two-phase transitions were observed; these authors also reported that the tetragonal-orthorhombic phase transition disappeared for a BT content of 6%. Men *et al.* [65 ~~61~~] also observed that for (1-x)KNN-xBT spark plasma sintered samples the shape of the permittivity peak became remarkably broadened for *x* higher than 4.

It could be possible to associate the real permittivity peaks broadening and their shifts to lower temperatures with the formation of vacancy complexes, specifically $V_A + V_O$ (where V_A could be V_{Na} or V_K), and to the creation of other kinds of point defects with associated big open volumes located at the orthorhombic-tetragonal phase boundaries. As mentioned above, this last kind of defects appears when the orthorhombic and tetragonal phases coexist and, therefore they could be linked to the stabilization of the polymorphic phase boundary with the composition change. As can be seen in Fig. 8, a notorious broadening in the permittivity *versus* temperature curve observed for the KNN-6BT sample is similar to that measured for the KNN-7BT sample. However, the XRD and PALS results presented in this work indicate that for the KNN-6BT sample the tetragonal and orthorhombic phases still coexist, although this last phase is the minority. These experimental proofs could be associated with the presence of nanoregions in which both the orthorhombic and tetragonal phases coexist in KNN ceramics containing until 6% BT. Interestingly, for samples with x=6% and 7% a hump at around ~350°C, which is associated with a residual KNN-phase slightly doped with

$BaTiO_3$, is observed. Although from the XRD patterns, the amount of this residual phase is lower than 2%, the sensitivity of dielectric properties makes it possible to detect it.

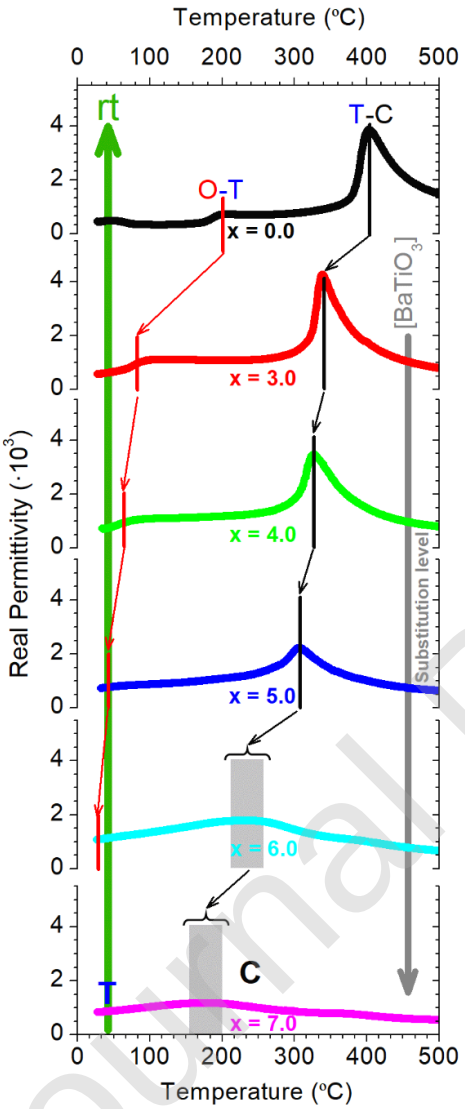

Figure 8. Temperature dependence of the real permittivity measured for the (100-x)$K_{0.5}Na_{0.5}NbO_3$-x$BaTiO_3$ ceramics at a frequency of 100 kHz (see details in the text).

For the sample containing the highest BT values; that is, sample KNN-7BT, the corresponding dielectric permittivity curve shows a significant flattening concerning the rest of the permittivity curves presented in Fig. 8. It must be pointed out that our PALS results

obtained for this sample indicate that positrons annihilate in vacancy-like defects located at the intergrain regions; that is, grain boundaries and in the intragrain regions (*e.g.*, point defects located inside the grains). In the last case, positrons annihilate in a defect state having mono- and/or di-cationic vacancies (V_{Na}, V_K, V_{Nb}) or in the intragrain bulk. The presence of the mentioned cationic vacancies inside the grains is compatible with, for instance, recently reported TEM results on the study of the (1-x)$K_{0.5}Na_{0.5}NbO_3$-x$SrZrO_3$ ($0.14 \leq x \leq 0.16$) ceramics, such results reveal the existence of an inhomogeneous element distribution from the shell to the core within grains [21]. Both effects could be responsible for the multi-peaks coupling resulting in a very diffuse peak as observed in Fig. 8. The diffuse phase transition has been observed in many ABO_3-type perovskites [66 ~~62~~] and, specifically, in $K_{0.5}Na_{0.5}NbO_3$-based ceramics [63]. As discussed above, due to the similar ionic radii, Ba^{2+} substitutes the A-site Na^+ and K^+, while Ti^{4+} substitutes the B-site Nb^{5+}. Therefore, the A- and B-sites show an inhomogeneous distribution of elements giving rise to a diffuse-phase transition [21,66,67 ~~62,63~~]. Moreover, the observed Raman bands broadening can also be associated with the enhancement of the diffuse-phase transition behavior of these ceramics with the BT addition. Our experimental results obtained for the KNN-7BT sample confirm that there is a progressive structural evolution from the orthorhombic to tetragonal symmetry correlated with an increase of the disorder degree with the addition of $BaTiO_3$.

On the other hand, it was found that the dielectric loss (tan δ) registers a strong reduction, with the barium titanate addition, across the complete temperature range studied (data not shown).

Finally, the small variation in the dielectric permittivity and the low dielectric loss (tan δ) across the wide temperature range from 25°C to 380°C observed for the KNN samples

having the highest $BaTiO_3$ additions suggest that these ceramics could be used for capacitors design with low capacitance variation in a wide temperature range [68 ~~64~~].

4. Conclusions

In the present work, the influence of the addition of barium titanate to lead-free (100-x)$K_{0.5}Na_{0.5}NbO_3$-x$BaTiO_3$ (x = 0, 3, 4, 5, 6 and 7) ceramics, prepared by a mechanochemically activated solid-state reaction synthesis method, on the structural changes at micro, nano, and sub-nanometric scale as well as the dielectric properties were studied.

From our investigations, it was possible to reveal that the BT addition to the KNN ceramic induces a progressive structural evolution from the orthorhombic crystal symmetry characteristic of pure KNN at RT to the tetragonal one; in fact, the KNN-$BaTiO_3$ samples presented a polymorphic behavior associated with the coexistence of the T and O phases. A systematic decrease of the grain size in the doped ceramics for increasing BT contents was also observed; specifically, from 2.4 μm (x=3) until 0.06 μm (x=7). Besides, the joint analysis of Raman spectroscopy and XRD made it possible to conclude that Ba^{2+} ions occupy the A-sites of the structure, while the Ti^{4+} ions replace the Nb^{5+} ions at the B-sites producing a distortion of the perovskite structure.

The use of PALS made it possible to reveal the nature of vacancy-like defects created during the O-T phase transitions, as well as the defect structure in each sample. In the case of the pure KNN ceramic characterized by a crystal symmetry entirely orthorhombic, it was found that in the defect structure there was a dominant kind of defects identified as $V_A + V_O$ complexes having a mean size comparable to that formed by two V_O surrounding one A-site vacancy. In the compositional range $3 \leq x \leq 6$, in the defect structure of the KNN-$BaTiO_3$

samples the same kind of vacancy complexes detected in the pure KNN sample were still mostly present; but the presence of big vacancy-like defects located at the orthorhombic-tetragonal phase boundaries was also detected. In the case of the sample containing the highest BT content; that is, x = 7 the defect structure is formed by small vacancy-like defects located in the intragrain regions with sizes comparable to a mono- or di-cationic vacancies (K and/or Na and/or Nb).

On the other hand, for the samples with BT concentrations between 3% and 6% the real permittivity peaks broadening and their shifts to lower temperatures observed during the orthorhombic to tetragonal phase transition were associated with the formation of the vacancy-like defects characterized by PALS.

An important result derived from the present work was that the use of a macroscopic analysis of the dielectric properties through, for instance, the dielectric permittivity *versus* temperature curves, cannot be used for the exact determination of the polymorphic phase transition. Conversely, PALS gave a clue to go deeper into the analysis of the XRD spectra obtained for the sample containing 6%; thus, it was found that still at such BT concentration the orthorhombic and tetragonal phases coexist as a consequence of the presence of minority orthorhombic nanoregions. This work opens a new way for the exact determination of the polymorphic phase transition in ceramics.

Acknowledgments

This work has been possible thanks to the economic and institutional support of the National Council of Scientific and Technical Research (CONICET), the National Agency for Scientific and Technological Promotion (ANPCyT-PICT 2015-1832), Comisión de Investigaciones Científicas de la Provincia de Buenos Aires (Argentina), Secretaría de

Ciencia, Arte y Tecnología – UNCPBA (Argentina), and the National University of Mar del Plata (UNMdP). Dr. F. Rubio-Marcos is also indebted to the MINECO (Spain) project MAT2017-86450-C4-1-R for their financial support. F.R-M. is grateful to MINECO for a 'Ramon y Cajal' contract (ref: RyC-2015-18626), which is co-financed by the European Social Fund. F.R-M. also acknowledges support from a 2018 Leonardo Grant for Researchers and Cultural Creators, BBVA Foundation.

Conflict of Interest

The authors declare that they have no conflict of interest.

Declaration of interests

The authors declare that they have no known competing financial interests or personal relationships that could have appeared to influence the work reported in this paper.

References

[1] K. Kakimoto, I. Masuda, H. Ohsato, Ferroelectric and Piezoelectric Properties of $KNbO_3$ Ceramics Containing Small Amounts of $LaFeO_3$, Jpn. J. Appl. Phys., 42 (2003) 6102-6105. https://doi.org/10.1143/JJAP.42.6102

[2] Y. Li, W. Chen, Q. Xu, J. Zhou, Y. Wang, H. Sun, Piezoelectric and dielectric properties of CeO_2-doped $Bi_{0.5}Na_{0.44}K_{0.06}TiO_3$ lead-free ceramics, Ceram. Int., 33 (2007) 95-99. https://doi.org/10.1016/j.ceramint.2005.08.001

[3] Z.-H. Zhao, Y. Dai, F. Huang, The formation and effect of defect dipoles in lead-free piezoelectric ceramics: A review, SM&T 20 (2019) e00092. https://doi.org/10.1016/j.susmat.2019.e00092

[4] T. Zheng, J. Wu, D. Xiao, J. Zhu, Recent development in lead-free perovskite piezoelectric bulk materials, Progress in Materials Science. 98 (2018) 552-624. https://doi.org/10.1016/j.pmatsci.2018.06.002

[5] Y. Saito, H. Takao, T. Tani, T. Nonoyama, K. Takatori, T. Homma, T. Nagaya, M. Nakamura, Lead-free piezoceramics, Nature 432 (2004) 84-87. https://doi.org/10.1038/nature03028

[6] J. Wu, D. Xiao, J. Zhu, Potassium−Sodium Niobate Lead-Free Piezoelectric Materials: Past, Present, and Future of Phase Boundaries Chem. Rev. 115 (2015) 2559-2595. https://doi.org/10.1021/cr5006809

[7] H.-C.Thong, C. Zhao, Z. Zhou. C.-F. Wu, Y.-X. Liu, Z.-Z. Du, J.-F. Li, W. Gong, Technology transfer of lead-free (K,Na)NbO_3-based piezoelectric ceramics, Mater. Today 29 (2019) 37-48. https://doi.org/10.1016/j.mattod.2019.04.016

[8] M.Adachi, K. Yan, K. Matsumoto, T. Karaki, Piezoelectric Properties of Modified $(K_{0.5}Na_{0.5})NbO_3$-$BaTiO_3$ Ceramics with the Mixture Sintering Aids of $0.6B_2O_3$-0.4CuO, Edinburgh, 20101-4. https://doi.org/10.1109/ISAF.2010.5712219.

[9] E. Hollenstein, D. Damjanovic, N. Setter, Temperature stability of the piezoelectric properties of Li-modified KNN ceramics, J. Eur. Ceram. Soc. 27 (2007) 4093-4097. https://doi.org/10.1016/j.jeurceramsoc.2007.02.100

[10] P. Palei, P. Kumar, Impedance Spectroscopy and AC Conductivity Studies of Ferroelectric $(K_{0.5}Na_{0.5})NbO_3$ Ceramics, J. Adv. Dielectr. 1 (2011) 351-356. https://doi.org/10.1142/S2010135X11000446

[11] H.-C.Thong, C. Zhao, Z.-X. Zhu, X. Chen, J.-F. Li, K. Wang, The impact of chemical heterogeneity in lead-free $(K,Na)NbO_3$ piezoelectric perovskite: Ferroelectric phase coexistence, Acta Mater. 166 (2019) 551-559. https://doi.org/10.1016/j.actamat.2019.01.012

[12] C.-W. Tao, X.-Y. Geng, J. Zhang, R.-X. Wang, Z.-B. Gu, S.-T. Zhang, $Bi_{0.5}Na_{0.5}TiO_3$-$BaTiO_3$-$K_{0.5}Na_{0.5}NbO_3$:ZnO relaxor ferroelectric composites with high breakdown electric field and large energy storage properties, J. Eur. Ceram. Soc. 38 (2018) 4946–4952. https://doi.org/10.1016/j.jeurceramsoc.2018.07.006[13] J. Hao, W. Li, J. Zhai, H. Chen, Progress in high-strain perovskite piezoelectric ceramics Materials Science and Engineering: R: Reports 135 (2019) 1-57. https://doi.org/10.1016/j.mser.2018.08.001

[14] K. Wang, J. F. Li, Analysis of crystallographic evolution in $(Na,K)NbO_3$-based lead-free piezoceramics by x-ray diffraction, Appl. Phys. Lett. 91 (2007) 262902. https://doi.org/10.1063/1.2825280

[15] Y. Guo, K. Kakimoto, H. Ohsato, Structure and Electrical Properties of Lead-Free $(Na_{0.5}K_{0.5})NbO_3$-$BaTiO_3$ Ceramics, Jpn. J. Appl. Phys. 43 (2004) 6662–6666. https://doi.org/10.1143/JJAP.43.6662

[16] H. Y. Park, C. W. Ahn, H. C. Song, J. H. Lee, S. Nahm, K. Uchino, H. G. Lee, H. J. Lee, Microstructure and piezoelectric properties of $0.95(Na_{0.5}K_{0.5})NbO_3$–$0.05BaTiO_3$ ceramics, Appl. Phys. Lett. 89 (2006) 062906. https://doi.org/10.1063/1.2335816

[17] C. W. Ahn, H. C. Song, S. Nahm, S. H. Park, K. Uchino, S. Priya, H. G. Lee, N. K. Kang, Effect of MnO_2 on the piezoelectric properties of $(1-x)(Na_{0.5}K_{0.5})NbO_3$-$xBaTiO_3$ ceramics, Jpn. J. Appl. Phys., 44 (2005) L1361–64. https://doi.org/10.1143/JJAP.44.L1361

[18] C. W. Ahn, C. S. Parka, D. Viehland, S. Nahm, D. H. Kang, K. S. Bae, S. Priya, Correlation between Phase Transitions and Piezoelectric Properties in Lead-Free $(K,Na,Li)NbO_3$-$BaTiO_3$ Ceramics, Jpn. J. Appl. Phys. 47 (2008) 8880–8883. https://doi.org/10.1143/JJAP.47.8880

[19] E. D. Politova, N. V. Golubko, G. M. Kaleva, A. V. Mosunov, N. V. Sadovskaya, S. Yu. Stefanovich, D. A. Kiselev, A. M. Kislyuk, P. K. Panda, Processing and characterization of lead-free ceramics on the base of sodium–potassium niobate, J. Adv. Dielectr. 8 (2018) 1850004. https://doi.org/10.1142/S2010135X18500042

[20] H. Cheng, W. Zhou, H. Du, F. Luo, D. Zhu, D. Jiang, B. Xu, Enhanced dielectric relaxor properties in $(1-x)(K_{0.5}Na_{0.5})NbO_3$–$x(Ba_{0.6}Sr_{0.4})_{0.7}Bi_{0.2}TiO_3$ lead-free ceramic, J. Alloy. Compd. 579 (2013) 192–197. https://doi.org/10.1016/j.jallcom.2013.06.077

[21] Liu, Z., Fan, H., Lei, S., Ren, X., Long, C., Duplex structure in $K_{0.5}Na_{0.5}NbO_3SrZrO_3$ ceramics with temperature-stable dielectric properties, J. Eur. Ceram. Soc. 37 (2017) 115–122. https://doi.org/10.1016/j.jeurceramsoc.2016.07.024

[22] Z. Liu, A. Zhang, J. Lu, B. Xie, B. Liang, Y. Mao, H. Fan, Balanced development of dielectric permittivity, loss tangent, and temperature stability in $K_{0.5}Na_{0.5}NbO_3$-based ceramic capacitors, J. Alloy. Compd. 817 (2020) 152798. https://doi.org/10.1016/j.jallcom.2019.152798

[23] P. Hautojärvi, C. Corbel, Positron spectroscopy of defects in metals and semiconductors, in Positron Spectroscopy of Solids, International School of Physics «Enrico Fermi», Course CXXV, A. Dupasquier, P. Mills Jr. (Eds.), IOS Press, Amsterdam, 1995, pp. 491-532.

[24] R. Krause-Rehberg, H.S. Leipner, Positron Annihilation in Semiconductors: Defect Studies, Springer Series in Solid State Science), Springer, Berlin 1999.

[25] F. Tuomisto, I. Makkonen, Defect identification in semiconductors with positron annihilation: Experiment and theory, Rev. Mod. Phys. 85 (2013), pp. 1583-1631. https://link.aps.org/doi/10.1103/RevModPhys.85.1583

[26] C. Macchi, A. Somoza, A. Dupasquier, A. López García, M. Castro, Positron trapping in $BaTiO_3$ perovskite J. Phys. Condens. Matter 13, (2001) 5717-5722. https://doi.org/10.1088/0953-8984/13/24/316

[27] M.S. Castro, W. Salgueiro, A. Somoza, Electron paramagnetic resonance and positron annihilation study of the compensation mechanisms in donor-doped $BaTiO_3$ ceramics, J. Phys. Chem. Solids 68 (2007) 1315-1323. https://doi.org/10.1016/j.jpcs.2007.02.017

[28] F. Rubio-Marcos, P. Marchet, J. J. Romero, J. F. Fernández, Structural, microstructural and electrical properties evolution of $(K,Na,Li)(Nb,Ta,Sb)O_3$ lead-free piezoceramics through NiO doping, J. Eur. Ceram. Soc. 31 (2011) 2309-2917. https://doi.org/10.1016/j.jeurceramsoc.2011.05.041

[29] J. Kansy, Microcomputer program for analysis of positron annihilation lifetime spectra, Nucl. Instrum. Meth. A 374 (1996) 235-244. https://doi.org/10.1016/0168-9002(96)00075-7

[30] F. Rubio-Marcos, M. A. Bañares, J. J. Romero, J. F. Fernandez, Correlation between the piezoelectric properties and the structure of lead-free KNN-modified ceramics, studied by Raman Spectroscopy, J. Raman Spectrosc. 42 (2011) 639-643. https://doi.org/10.1002/jrs.2753

[31] R. Singh, K. Kambale, A. R. Kulkarni, C. S. Harendranath, Structure composition correlation in KNN–BT ceramics – An X-ray diffraction and Raman spectroscopic investigation, Mater. Chem. Phys. 138 (2013) 905-908. https://doi.org/10.1016/j.matchemphys.2012.12.082

[32] X. Ren, Z. Peng, B. Chen, Q. Shi, X. Qiao, D. Wu, G. Li, , Z. Yang, X. Chao, A compromise between piezoelectricity and transparency in KNN-based ceramics: The dual functions of Li_2O addition, J. Eur. Ceram. Soc. 40 (2020) 2331-2337. https://doi.org/10.1016/j.jeurceramsoc.2020.01.029

[33] J. Hreščak, G. Dražić, M. Deluca, I. Arčon, A. Kodre, M. Dapiaggi, T. Rojac, B. Malič, A. Bencan, Donor doping of $K_{0.5}Na_{0.5}NbO_3$ ceramics with strontium and its implications to grain size, phase composition and crystal structure, J. Eur. Ceram. Soc., 37 (2017) 2073-2082. https://doi.org/10.1016/j.jeurceramsoc.2016.12.053

[34] K. Kakimoto, K. Akao, Y. Guo, H. Ohsato, Raman Scattering Study of Piezoelectric $(Na_{0.5}K_{0.5})NbO_3$-$LiNbO_3$ Ceramics, Jpn. J. Appl. Phys. 44 (2005) 7064. https://doi.org/10.1143/JJAP.44.7064.

[35] M. Połomska, B. Hilczer, M. Kosec, and B. Malič, Raman Scattering Studies of Lead Free $(1-x)K_{0.5}Na_{0.5}NbO_3$-$xSrTiO_3$ Relaxors, Ferroelectrics 369 (2008) 149-156 https://doi.org/10.1080/00150190802374873

[36] D. Lin, K.W. Kwok, H. Chan, Structure, Dielectric, and Piezoelectric Properties of CuO-doped $K_{0.5}Na_{0.5}NbO_3$–$BaTiO_3$ Lead-Free Ceramics. Journal of Applied Physics – J. Appl. Phys. 102 (2007) 074113. https://doi.org/10.1063/1.2787164.

[37] Tian-Lu, Fang-Zhou Yao, Zhi-Xiang Zhu, Ke Wang, Jing-Feng Li, Piezoelectric properties of $(K_{0.5}Na_{0.5})NbO_3$-$BaTiO_3$ lead-free ceramics prepared by spark plasma sintering, J. Adv. Dielectr. 6 (2016) 1650013. https://doi.org/10.1142/S2010135X16500132

[38] J. König, M. Spreitzer, B. Jančar, D. Suvorov, Z. Samardžija, A. Popovič, The thermal decomposition of $K_{0.5}Bi_{0.5}TiO_3$ ceramics, J. Eur. Ceram. Soc. 29 (2009) 1695-1701. https://doi.org/10.1016/j.jeurceramsoc.2008.10.002

[39] H. Wei, H. Wang, Y. Xia, D. Cui, Y. Shi, M. Dong, C. Liu, T. Ding, J. Zhang, Y. Ma, N. Wang, Z. Wang, Y. Sun, R. Wei, Z. Guo, An overview of lead-free piezoelectric materials and devices, J. Mater. Chem. C, 6 (2018)12446-12467. https://doi.org/10.1039/C8TC04515A

[40] J.-F. Li, K. Wang, F.-Y. Zhu, L.-Q. Cheng, F.-Z. Yao, K,Na)NbO_3-Based Lead-Free Piezoceramics: Fundamental Aspects, Processing Technologies, and Remaining Challenges, J. Am. Ceram. Soc. 96 (2013) 3677-3696. https://doi.org/10.1111/jace.12715

[41] J. Wu, D. Xiao, J. Zhu, Potassium-sodium niobate lead-free piezoelectric materials: past, present, and future of phase boundaries, Chem. Rev. 115 (2015) 2559-95 https://doi.org/10.1021/cr5006809

[42] B. Ponraj, K. B. R. Varma, Enhancement in the physical properties of $K_{0.5}Na_{0.5}NbO_3$ ceramics by the addition of 0.5 Li_2O – 0.5K_2O – 2B_2O_3 glass, Integr. Ferroelectr., 176 (2016) 257-267, https://doi.org/10.1080/10584587.2016.1252659

[43 ~~39~~] M. A. M. Hatta, M. W. A. Rashid, U. A.-A. H. Azlan, N. A. Azmi, M. A. Azam, T. Moriga, Influence of Yttrium Dopant on the Structure and Electrical Conductivity of

Potassium Sodium Niobate Thin Films, Mater. Res. 19 (2016) 1417-1422. https://doi.org/10.1590/1980-5373-mr-2016-0076

[44 ~~40~~] M. A. Rafiq, M. E. Costa, A. Tkach, P. M. Vilarinho, Impedance Analysis and Conduction Mechanisms of Lead Free Potassium Sodium Niobate (KNN) Single Crystals and Polycrystals: A Comparison Study, Cryst. Growth Des. 15 (2015) 1289-1294. https://doi.org/10.1021/cg5016884

[45 ~~41~~] A. Polity, R. Krause-Rehberg, T.E.M. Staab, M.J. Puska, J Klais, H.J. Möller, B. K. Meyer, Study of defects in electron irradiated $CuInSe_2$ by positron lifetime spectroscopy. Journal of Applied Physics. 83 (1998) 71-78. https://doi.org/10.1063/1.366703

[46 ~~42~~] C. Macchi, C. Maurizio, R. Checchetto, S. Mariazzi, L. Ravelli, W. Egger, P. Mengucci, N. Bazzanella, A. Miotello, A. Somoza, R. S. Brusa, Niobium aggregation and vacancy-like defect evolution in nanostructured Nb-doped Mg: Their role in the kinetics of the hydride-to-metal phase transformation, Phys. Rev. B 85 (2012) 214117: 1-19. https://link.aps.org/doi/10.1103/PhysRevB.85.214117

[47 ~~43~~] M. J. Puska, R. M. Nieminen, Theory of positrons in solids and on solid surfaces. Rev Mod Phys. 66 (1994) 841-897. https://link.aps.org/doi/10.1103/RevModPhys.66.841

[48 ~~44~~] T. Torsti, T. Eirola, J. Enkovaara, T. Hakala, P. Havu, V. Havu, T. Höynälänmaa, J. Ignatius, M. Lyly, I. Makkonen, T. T. Rantala, J. Ruokolainen, K. Ruotsalainen, E. Räsänen, H. Saarikoski, M. J. Puska, Three real-space discretization techniques in electronic structure calculations. Phys. Status Solidi B 243 (2006) 1016–1053 https://doi.org/10.1002/pssb.200541348

[49 ~~45~~] E. Boronski, R.M. Nieminen, Electron-positron density-functional theory, Phys. Rev B. 34 (1986) 3820-3831. https://link.aps.org/doi/10.1103/PhysRevB.34.3820

[50 ~~46~~] M.J. Puska,S. Mäkinen, M. Manninen, R.M. Nieminen, Screening of positrons in semiconductors and insulators, Phys. Rev. B. 39 (1989) 7666-7679. https://link.aps.org/doi/10.1103/PhysRevB.39.7666

[51 ~~47~~] A. Jain, S.P. Ong, G. Hautier, W. Chen, W.D. Richards, S. Dacek, S. Cholia, D. Gunter, D. Skinner, G. Ceder, K.A. Persson, The Materials Project: A materials genome approach to accelerating materials innovation, APL Materials 1 (2013) 011002-1-11. http://dx.doi.org/10.1063/1.4812323

[52 ~~48~~] T. Wang, L. He, Y. Deng, Q. Zheng, Q. Li, N. Jiang, C. Xu, X. Cao, D. Lin, Origin of superior hardening properties in $KCuTa_3O_9$-doped $K_{0.5}Na_{0.5}NbO_3$ lead-free piezoelectric ceramics, Ceram. Int. 43 (2017) 15666–15677. https://doi.org/10.1016/j.ceramint.2017.08.126

[53 ~~49~~] S. Dwivedi, T. Pareek, S. Kumar, Structure, dielectric, and piezoelectric properties of $K_{0.5}Na_{0.5}NbO_3$-based lead-free ceramics, RSC Adv. 8 (2018) 24286-24296. https://doi.org/10.1039/C8RA04038A

[54 ~~50~~] D. J. Keeble, S. Wicklein, R. Dittmann, L. Ravelli, R. A. Mackie, W. Egger, Identification of A- and B-Site Cation Vacancy Defects in Perovskite Oxide Thin Films, Phys. Rev. Lett. 105 (2010) 226102. https://doi.org/10.1103/PhysRevLett.105.226102

[55 ~~51~~] P. Ctibor, J. Čížek, J. Sedláček, F. Lukáč, Dielectric properties and vacancy-like defects in plasma-sprayed barium titanate, J. Am. Ceram. Soc. 100 (2017) 2972-2983. https://doi.org/10.1111/jace.14840

[56 ~~52~~] Y. Zhen, J.F. Li, Normal sintering of $(K,Na)NbO_3$-based ceramics: influence of sintering temperature on densification, microstructure, and electrical properties, J. Am. Ceram. Soc. 89 (2006) 3669–3675. https://doi.org/10.1111/j.1551-2916.2006.01313.x

[57 ~~53~~] J. Čížek, O. Melikhova, I. Procházka, J. Kuriplach, R. Kužel, G. Brauer, W. Anwand, T. E. Konstantinova, I. A. Danilenko, Defect studies of nanocrystalline zirconia powders and sintered ceramics, Phys. Rev. B 81 (2010) 024116. https://link.aps.org/doi/10.1103/PhysRevB.81.024116

[58 ~~54~~] C.Macchi, M.A. Ponce, P.M. Desimone. C. M. Aldao, A. Somoza, Vacancy-like defects in nanocrystalline SnO_2: influence of the annealing treatment under different atmospheres, Philos. Mag. 98 (2018) 673-692. https://doi.org/10.1080/14786435.2017.1415466

[59 ~~55~~] H.E. Schaefer, R. Würschum, R. Birringer, H. Gleiter, Structure of nanometer-sized polycrystalline iron investigated by positron lifetime spectroscopy, Phys. Rev. B 38 (1988) 9545-9554. https://doi.org/10.1103/physrevb.38.9545

[60 ~~56~~] R. Checchetto, N. Bazzanella, A. Kale, A. Miotello, S. Mariazzi, R.S. Brusa, P. Mengucci, C. Macchi, A. Somoza A, W. Egger, L. Ravelli, Enhanced kinetics of hydride-metal phase transition in magnesium by vacancy clustering, 2011 Phys. Rev. B 84 (2011) 054115:1- 7. https://link.aps.org/doi/10.1103/PhysRevB.84.054115

[61 ~~57~~] A. Dupasquier, R. Romero, A. Somoza, Positron trapping at grain boundaries, Phys. Rev. B 48 (1993) 9235-9245. https://link.aps.org/doi/10.1103/PhysRevB.48.9235

[62 ~~58~~] D. W. Baker, P. A. Thomas, N. Zhang, A. M. Glazer, Structural study of $K_xNa_{1-x}NbO_3$ (KNN) for compositions in the range x = 0.24-0.36, Acta Cryst. B 65 (2009) 22-28. https://doi.org/10.1107/S0108768108037361

[63 ~~59~~] M. Acosta, N. Novak, V. Rojas, S. Patel, R. Vaish, J. Koruza, G.A. Rossetti, J. Rödel, $BaTiO_3$-based piezoelectrics: Fundamentals, current status, and perspectives. Appl. Phys. Rev. 4 (2017) 041305. https://doi.org/10.1063/1.4990046

[64 ~~60~~] X. Chen, Y. Wang, J. Chen, H. Zhou, L. Fang, L. Liu, Dielectric Properties and Impedance Analysis of $K_{0.5}Na_{0.5}NbO_3$-$Ba_2NaNb_5O_{15}$ Ceramics with Good Dielectric Temperature Stability. J. Am. Ceram. Soc. 96 (2013) 3489–3493. https://doi.org/10.1111/jace.12514

[65 ~~61~~] T.-L. Men, F.-Z. Yao, Z.-X. Zhu, K. Wang, J.-F. Li, Piezoelectric properties of $(K_{0.5}Na_{0.5})NbO_3$-$BaTiO_3$ lead-free ceramics prepared by spark plasma sintering J. Adv. Dielectr. 6 (2016) 1650013. https://doi.org/10.1142/S2010135X16500132

[66 ~~62~~] Z. Raddaoui, S. El Kossi, J. Dhahri, N. Abdelmoulab, K. Taibic, Study of diffuse phase transition and relaxor ferroelectric behavior of $Ba_{0.97}Bi_{0.02}Ti_{0.9}Zr_{0.05}Nb_{0.04}O_3$ ceramic, RSC Adv. 9 (2019) 2412–2425. https://doi.org/10.1039/c8ra08910h

[67 ~~63~~] Lin, D., Kwok, K. W., & Chan, H. L. W. (2007). Structure, dielectric, and piezoelectric properties of CuO-doped $K_{0.5}Na_{0.5}NbO_3$–$BaTiO_3$ lead-free ceramics. J. Appl. Phys. 102 (2007) 074113. https://doi.org/10.1063/1.2787164

[68 ~~64~~] R. Muhammad, J. Camargo, A. Prado, M. S. Castro, Temperature stable relative permittivity from −60 to 200 °C in $75BaTiO_3$–$(25-x)BiMg_{0.5}Ti_{0.5}O_3$–$xNaNbO_3$ ceramics with X9R like characteristics, Mater. Lett. 233 (2018) 258-262. https://doi.org/10.1016/j.matlet.2018.09.022